PHYSICAL REVIEW D **88,** 073003 (2013)

# Study on perturbation schemes for achieving the real PMNS matrix from various symmetric textures

Bin Wang,[1] Jian Tang,[2] and Xue-Qian Li[1]

[1]*School of Physics, Nankai University, Tianjin 300071, China*

[2]*Center for Particle Physics, University of Alberta, Edmonton, Alberta, T6G 2E1 Canada*

(Received 8 March 2013; published 14 October 2013)

The Pontecorvo-Maki-Nakawaga-Sakata matrix displays an obvious symmetry but not exact. There are several textures proposed in the literature which possess various symmetry patterns and seem to originate from different physics scenarios at high energy scales. To be consistent with the experimental measurement, however, the symmetry must be broken. Following the schemes given in the literature, we modify the matrices (ten in total) to gain the real Pontecorvo-Maki-Nakawaga-Sakata matrix by perturbative rotations. The results may be useful for future model builders.

DOI: 10.1103/PhysRevD.88.073003 PACS numbers: 14.60.Pq

## I. INTRODUCTION

Mixing among fermions is one of the most mysterious aspects in particle physics. Mixing among leptons displays an obvious regularity but not equal to the identity of the quark mixing. It is well known that the mixing among fermions originates from the fact that the weak eigenstates of fermions (quarks and leptons) are not that of the mass Hamiltonian, and the rotation from the weak basis to the mass basis results in the mixing matrix [1]. As is observed, the structures of the quark and lepton mixing matrices are so different, and it implies that the mechanisms which determine their mass eigenstates would be different. Lam suggests that a higher horizontal symmetry $U(1) \times SO(3)$ is broken into the tetrahedral $A_4$ and nematic $Z_2 \times Z_2 \times Z_2$ sectors which correspond to the lepton and quark mixing, respectively [2]. Definitely, it is only one of the possible structures which were discussed in the literature. It is believed that there must be a higher symmetry at high energy scales, and later it is broken during the evolution from high energy to the weak energy scale. It is worth pointing out that Lam's mechanism which determines an $A_4$ symmetry for the lepton mixing demands $\theta_{13}$ in the mixing matrix to be zero. And most of the proposed symmetries would result in the same zero $\theta_{13}$. However, the recent experiments of the T2K [3], Double-Chooz [4,5], Daya-Bay [6–8], and RENO [9] Collaborations all confirm that $\theta_{13}$ is not zero but sizable as near 9°. This implies that, even though the lepton mixing matrix displays an approximate symmetric form, its original symmetry must be broken.

The most plausible way to break the symmetry is to perturb the matrix to realize a practical lepton mixing matrix which is obtained by fitting the data while the unitarity of the matrix must be retained. The form of the perturbation may hint to us the breaking mechanism which is important for understanding the nature. Moreover, in the process of perturbing the matrix and comparing with data, we notice that several textures of the matrix are disfavored or marginally favored, even though a perturbative rotation would make them in marginal agreement with data (see the text). That is the breaking mechanism. A careful analysis of the breaking (indeed the perturbation) indicates that one may have an opportunity to realize what original symmetric texture(s) is more realistic, so one would be able to trace back to high energy scale physics where the mixing originates. In particular, such a study about the patterns of perturbation may be useful for future model builders.

As is well known, nonzero neutrino masses, neutrino or lepton mixing, and relatively small splitting among neutrino masses are the three conditions leading to the quantum mechanical phenomena: observable neutrino oscillations [10,11]. The mixing matrix in the lepton sector $U_L^\dagger U_R$ ($U_L$ and $U_R$ take part in the diagonalizations of charged lepton and neutrino mass matrices, respectively) are named as the Pontecorvo-Maki-Nakawaga-Sakata (PMNS) [12,13] matrix

$$U_{\rm PMNS} = U_L^\dagger U_R, \tag{1}$$

which is a $3 \times 3$ unitary matrix and can be parameterized via mixing angles $\theta_{12}$, $\theta_{23}$, and $\theta_{13}$ and one $CP$ phase $\delta$ [10]:

$$U_{\rm PMNS} = \begin{pmatrix} c_{12}c_{13} & s_{12}c_{13} & s_{13}e^{-i\delta} \\ -s_{12}c_{23} - c_{12}s_{23}s_{13}e^{i\delta} & c_{12}c_{23} - s_{12}s_{23}s_{13}e^{i\delta} & s_{23}c_{13} \\ s_{12}s_{23} - c_{12}c_{23}s_{13}e^{i\delta} & -c_{12}s_{23} - s_{12}c_{23}s_{13}e^{i\delta} & c_{23}c_{13} \end{pmatrix}, \tag{2}$$

where $c_{ij} \equiv \cos\theta_{ij}$, $s_{ij} \equiv \sin\theta_{ij}$. If neutrinos are Majorana particles, there could be one additional matrix $\mathrm{diag}(e^{\alpha_1/2}, e^{\alpha_2/2}, 1)$, and since it is not revelent to neutrino oscillations at all, we ignore it in this work. The mixing angles and Jarlskog invariant $J_{CP}$, which determines the magnitude of $CP$ violation in neutrino oscillation [10,14,15], are

 

TABLE I. The updated global fit results of three neutrino oscillation, where $\Delta m^2$ is defined as $m_3^2 - (m_1^2 + m_2^2)/2$ and $\delta m^2 = m_2^2 - m_1^2$.

| Parameter | Best fit | $1\sigma$ range | $2\sigma$ range | $3\sigma$ range |
|---|---|---|---|---|
| $\delta m^2/10^{-5}$ eV$^2$ (NH or IH) | 7.54 | 7.32–7.80 | 7.15–8.00 | 6.99–8.18 |
| $\sin^2\theta_{12}/10^{-1}$ (NH or IH) | 3.07 | 2.91–3.25 | 2.75–3.42 | 2.59–3.59 |
| $\Delta m^2/10^{-3}$ eV$^2$ (NH) | 2.43 | 2.33–2.49 | 2.27–2.55 | 2.19–2.62 |
| $\Delta m^2/10^{-3}$ eV$^2$ (IH) | 2.42 | 2.31–2.49 | 2.26–2.53 | 2.17–2.61 |
| $\sin^2\theta_{13}/10^{-2}$ (NH) | 2.41 | 2.16–2.66 | 1.93–2.90 | 1.69–3.13 |
| $\sin^2\theta_{13}/10^{-2}$ (IH) | 2.44 | 2.19–2.67 | 1.94–2.91 | 1.71–3.15 |
| $\sin^2\theta_{23}/10^{-1}$ (NH) | 3.86 | 3.65–4.10 | 3.48–4.48 | 3.31–6.37 |
| $\sin^2\theta_{23}/10^{-1}$ (IH) | 3.92 | 3.70–4.31 | 3.53–4.84 ⊕ 5.43–6.41 | 3.35–6.63 |
| $\delta/\pi$ (NH) | 1.08 | 0.77–1.36 | ⋯ | ⋯ |
| $\delta/\pi$ (IH) | 1.09 | 0.83–1.47 | ⋯ | ⋯ |

$$T_{12} \equiv \tan\theta_{12} = \frac{|U_{e2}|}{|U_{e1}|}, \tag{3}$$

$$T_{23} \equiv \tan\theta_{23} = \frac{|U_{\mu 3}|}{|U_{\tau 3}|}, \tag{4}$$

$$S_{13} \equiv \sin\theta_{13} = |U_{e3}|, \tag{5}$$

$$J_{CP} \equiv \mathrm{Im}(U_{\mu 3} U_{e3}^* U_{e2} U_{\mu 2}^*). \tag{6}$$

The recent data indicate that the angle $\theta_{13}$ is sizable:

(i) *KamLAND.*—Global $\theta_{13}$ analysis incorporating CHOOZ, atmospheric, and long-baseline accelerator experiments indicates $\sin^2\theta_{13} = 0.009^{+0.013}_{-0.007}$ (i.e., $\theta_{13} = 5.444^{+3.086}_{-2.881}{}^\circ$) and nonzero $\theta_{13}$ at 79% C.L. [16].

(ii) *T2K.*—At 90% C.L. and for $\delta_{CP} = 0$, $4.99^\circ(5.77^\circ) < \theta_{13} < 15.97^\circ(17.83^\circ)$ for normal (inverted) hierarchy [3].

(iii) *MINOS.*—With $\delta_{CP} = 0$ the best fit result is $2\sin^2\theta_{23}\sin^2\theta_{13} = 0.041^{+0.047}_{-0.031}(0.079^{+0.071}_{-0.053})$ for normal (inverted) hierarchy and $\theta_{13} = 0$ is disfavored at 89% C.L. [17].

(iv) *Double Chooz.*—The early result from the Double Chooz reactor electron antineutrino disappearance experiment is $3.7^\circ < \theta_{13} < 12^\circ$ at 90% C.L. [4]. The updated results are $\sin^2 2\theta_{13} = 0.109 \pm 0.030(\mathrm{stat}) \pm 0.025(\mathrm{syst})$ (i.e., the central value $\theta_{13} = 9.639^\circ$) and excluding the no-oscillation hypothesis at 99.8% C.L. [5].

(v) *DayaBay.*—The Daya Bay Collaboration presents the reactor electron antineutrino disappearance experiment result $\sin^2 2\theta_{13} = 0.092 \pm 0.016(\mathrm{stat}) \pm 0.005(\mathrm{syst})$ (i.e., the central value $\theta_{13} = 8.8^\circ$) and nonzero $\theta_{13}$ with a significance of 5.2 standard deviations [6]. The recent updated result is $\sin^2 2\theta_{13} = 0.089 \pm 0.010(\mathrm{stat}) \pm 0.005(\mathrm{syst})$ (i.e., the central value $\theta_{13} = 8.7^\circ$) with $\theta_{13} = 0$ disfavored at $7.7\sigma$ [7,8].

(vi) *RENO.*—The result from the RENO experiment is $\sin^2 2\theta_{13} = 0.113 \pm 0.013(\mathrm{stat}) \pm 0.019(\mathrm{syst})$ (i.e., the central value $\theta_{13} = 9.821^\circ$) [9].

For convenience of discussion, an updated global analysis on neutrino oscillation data [18] is represented in Table I, and we single out the mixing angles and represent them in degrees in Table II, where NH and IH stand for cases of normal hierarchy and inverted hierarchy, respectively.

Analyzing the PMNS matrix, one notices an obvious symmetry but not exact. If writing it in an ideal form which has an exact symmetry, there are various textures which have different symmetric patterns. In other words, some phenomenologically assigned forms for the mixing matrix $U_{\mathrm{PMNS}}$ explicitly manifest flavor symmetries, while the practical form of the matrix implies that the symmetric structures should be spontaneously or explicitly broken. By synthesizing the proposals for the symmetric textures existing in the literature, there are ten in total such *Ansätze*:

TABLE II. The mixing angles from neutrino oscillation fit results in [18] (in degree).

| Parameter | Best fit | $1\sigma$ range | $2\sigma$ range | $3\sigma$ range |
|---|---|---|---|---|
| $\theta_{12}$ (NH or IH) | 33.6 | 32.6–34.8 | 31.6–35.8 | 30.6–36.8 |
| $\theta_{13}$ (NH) | 8.93 | 8.45–9.39 | 7.99–9.80 | 7.47–10.2 |
| $\theta_{13}$ (IH) | 8.99 | 8.51–9.40 | 8.01–9.82 | 7.51–10.2 |
| $\theta_{23}$ (NH) | 38.4 | 37.2–39.8 | 36.2–42.0 | 35.1–53.0 |
| $\theta_{23}$ (IH) | 38.8 | 37.5–41.0 | 36.5–42.0 ⊕ 47.5–53.2 | 35.4–54.5 |
| $\delta$ (NH) | 194.4 | 138.6–244.8 | ⋯ | ⋯ |
| $\delta$ (IH) | 196.2 | 149.4–264.6 | ⋯ | ⋯ |

(i) tribimaximal mixing (TBM) [19]; (ii) democratic mixing (DM) [20]; (iii) bimaximal mixing (BM) [21]; (iv) golden ratio mixing 1 (GRM1) [22]; (v) golden ratio mixing 2 (GRM2) [23]; (vi) hexagonal mixing (HM) [24]; (vii) tetramaximal mixing (TMM) [25]; (viii) Toorop-Feruglio-Hagedorn mixing 1 (TFH1) [26–28]; (ix) Toorop-Feruglio-Hagedorn mixing 2 (TFH2) [26–28]; (x) bidodeca mixing (BDM) [29]. We list the explicit forms of these patterns in Sec. II.

Some of the matrix forms listed above require zero $\theta_{13}$ which is in obvious contradiction to the newly measured value. It is shown that all those forms can be modified with perturbative rotations into the form of a real PMNS matrix which is consistent with the data.

In this work, we explicitly show how a perturbative rotation transforms the matrix into the one with a sizable $\theta_{13}$ and practical $\theta_{12}$ and $\theta_{23}$. Our numerical analyses are shown via several tables and figures. Then we present some discussions in the last section.

## II. THE SYMMETRIC TEXTURES OF THE MIXING MATRIX

Here we list all ten symmetric textures proposed in the literature:

$$U_{\rm TBM} = \begin{pmatrix} \sqrt{\frac{2}{3}} & \frac{1}{\sqrt{3}} & 0 \\ -\frac{1}{\sqrt{6}} & \frac{1}{\sqrt{3}} & \frac{1}{\sqrt{2}} \\ \frac{1}{\sqrt{6}} & -\frac{1}{\sqrt{3}} & \frac{1}{\sqrt{2}} \end{pmatrix}, \tag{7}$$

$$U_{\rm DM} = \begin{pmatrix} \frac{1}{\sqrt{2}} & \frac{1}{\sqrt{2}} & 0 \\ -\frac{1}{\sqrt{6}} & \frac{1}{\sqrt{6}} & \sqrt{\frac{2}{3}} \\ \frac{1}{\sqrt{3}} & -\frac{1}{\sqrt{3}} & \frac{1}{\sqrt{3}} \end{pmatrix}, \tag{8}$$

$$U_{\rm BM} = \begin{pmatrix} \frac{1}{\sqrt{2}} & \frac{1}{\sqrt{2}} & 0 \\ -\frac{1}{2} & \frac{1}{2} & \frac{1}{\sqrt{2}} \\ \frac{1}{2} & -\frac{1}{2} & \frac{1}{\sqrt{2}} \end{pmatrix}, \tag{9}$$

$$U_{\rm GRM1} = \begin{pmatrix} \sqrt{\frac{1}{2}\left(1+\frac{1}{\sqrt{5}}\right)} & \sqrt{\frac{2}{5+\sqrt{5}}} & 0 \\ -\frac{1}{\sqrt{5+\sqrt{5}}} & \frac{1}{2}\sqrt{1+\frac{1}{\sqrt{5}}} & \frac{1}{\sqrt{2}} \\ \frac{1}{\sqrt{5+\sqrt{5}}} & -\frac{1}{2}\sqrt{1+\frac{1}{\sqrt{5}}} & \frac{1}{\sqrt{2}} \end{pmatrix}, \tag{10}$$

$$U_{\rm GRM2} = \begin{pmatrix} \frac{1}{4}(1+\sqrt{5}) & \frac{1}{2}\sqrt{\frac{1}{2}(5-\sqrt{5})} & 0 \\ -\frac{1}{4}\sqrt{5-\sqrt{5}} & \frac{1+\sqrt{5}}{4\sqrt{2}} & \frac{1}{\sqrt{2}} \\ \frac{1}{4}\sqrt{5-\sqrt{5}} & -\frac{1+\sqrt{5}}{4\sqrt{2}} & \frac{1}{\sqrt{2}} \end{pmatrix}, \tag{11}$$

$$U_{\rm HM} = \begin{pmatrix} \frac{\sqrt{3}}{2} & \frac{1}{2} & 0 \\ -\frac{1}{2\sqrt{2}} & \frac{1}{2}\sqrt{\frac{3}{2}} & \frac{1}{\sqrt{2}} \\ \frac{1}{2\sqrt{2}} & -\frac{1}{2}\sqrt{\frac{3}{2}} & \frac{1}{\sqrt{2}} \end{pmatrix}, \tag{12}$$

$$U_{\rm TMM} = \begin{pmatrix} \frac{1}{2}\left(1+\frac{1}{\sqrt{2}}\right) & \frac{1}{2} & \frac{1}{2}\left(1-\frac{1}{\sqrt{2}}\right) \\ -\frac{1-i(1-\sqrt{2})}{2\sqrt{2}} & \frac{1}{2}\left(1-\frac{i}{\sqrt{2}}\right) & \frac{1+i(1+\frac{1}{\sqrt{2}})}{2\sqrt{2}} \\ \frac{1+i(1-\sqrt{2})}{2\sqrt{2}} & -\frac{1}{2}\left(1+\frac{i}{\sqrt{2}}\right) & -\frac{1-i(1+\frac{1}{\sqrt{2}})}{2\sqrt{2}} \end{pmatrix}, \tag{13}$$

$$U_{\rm TFH1} = \begin{pmatrix} \frac{3+\sqrt{3}}{6} & \frac{1}{\sqrt{3}} & \frac{-3+\sqrt{3}}{6} \\ \frac{-3+\sqrt{3}}{6} & \frac{1}{\sqrt{3}} & \frac{3+\sqrt{3}}{6} \\ \frac{1}{\sqrt{3}} & -\frac{1}{\sqrt{3}} & \frac{1}{\sqrt{3}} \end{pmatrix}, \tag{14}$$

$$U_{\rm TFH2} = \begin{pmatrix} \frac{3+\sqrt{3}}{6} & \frac{1}{\sqrt{3}} & \frac{3-\sqrt{3}}{6} \\ -\frac{1}{\sqrt{3}} & \frac{1}{\sqrt{3}} & \frac{1}{\sqrt{3}} \\ \frac{3-\sqrt{3}}{6} & -\frac{1}{\sqrt{3}} & \frac{3+\sqrt{3}}{6} \end{pmatrix}, \tag{15}$$

$$U_{\rm BDM} = \begin{pmatrix} \cos\frac{\pi}{6} & \sin\frac{\pi}{6} & 0 \\ -\frac{1}{\sqrt{2}}\sin\frac{\pi}{6} & \frac{1}{\sqrt{2}}\cos\frac{\pi}{6} & -\frac{1}{\sqrt{2}} \\ -\frac{1}{\sqrt{2}}\sin\frac{\pi}{6} & \frac{1}{\sqrt{2}}\cos\frac{\pi}{6} & \frac{1}{\sqrt{2}} \end{pmatrix}. \tag{16}$$

It is noted that our expressions of the symmetric forms listed above may differ from those given in the literature by a sign or even a phase factor in a row or column of the matrices, but, obviously, an additional overall phase $e^{i\alpha}$ does not change the physics of the mixing, and, moreover, our forms are more convenient to be compared with the conventional expression Eq. (2) adopted by the Particle Data Group [10].

## III. THE MINIMAL MODIFICATIONS TO THESE PATTERNS

As is well known, the eigenstates of weak interaction are not that of the mass Hamiltonian; thus, for physical processes one should rotate the weak basis into the mass basis. The unitary transformation between the two bases is expressed as a $3 \times 3$ matrix: the Cabibbo-Kobayashi-Maskawa (CKM) matrix for quarks and the PMNS matrix

for leptons. The PMNS matrix manifests a not-exact regulation. It is supposed that the exact symmetric texture is originating from a symmetry at a high energy scale, and breaking it leads to the practical matrix which keeps an approximate symmetric pattern.

Our goal is to break the symmetric matrix by a perturbation.

For that, the mass differences among quarks are very large, and there exists no regularity in the quark sector, as is shown in Wolfenstein's parametrization [30]; i.e., the quark mixing matrix is identity at the first order and is corrected by $\mathcal{O}(\lambda)$:

$$\begin{pmatrix} 1 & \lambda & \lambda^3 \\ \lambda & 1 & \lambda^2 \\ \lambda^3 & \lambda^2 & 1 \end{pmatrix}. \tag{17}$$

The mass differences in charged leptons are also relatively large; then the corresponding unitary matrices diagonalizing the charged lepton mass matrix would also demonstrate the above Wolfenstein-like form. For neutrinos, with the latest Planck data [31] $\sum m_\nu < 0.23$ eV and squared-mass differences from Particle Data Group [10] $\Delta m^2_{21} = (7.50 \pm 0.20) \times 10^{-5}$ eV$^2$, $|\Delta m^2_{32}| = (2.32^{+0.12}_{-0.08}) \times 10^{-3}$ eV$^2$, it is apparent that the mass differences among $\nu_1$, $\nu_2$, and $\nu_3$ are very small. It can be concluded that the neutrino sector contributes most to the lepton mixing. In addition, the mixing parameters between quark and lepton sectors are correlated by some empirical formulas, for instance, the quark-lepton complementarity [32] and $\theta_{13} = \theta_C/\sqrt{2}$ [33], with $\theta_C$ being the Cabibbo angle.

Unlike the mixing matrix for quarks $U_{\mathrm{CKM}}$, which does not show any symmetry, $U_{\mathrm{PMNS}}$ demonstrates an approximate symmetry, for example, the TBM texture and others listed in this work. Even though in the literature, the symmetry (approximate) is determined by a symmetry group such $A_4$, etc., from the physics picture, we should think that some symmetry exists in the mass matrices of charged leptons and neutrinos. One can further consider that the high symmetry might exist at a high energy scale, say, the seesaw scale, but is broken during the evolution to a lower energy scale (for example, the $\mu - \tau$ symmetry [34]). That breaking mechanism must apply to the mass matrices of both charged leptons and neutrinos. We suppose that diagonalizing the original mass matrices of charged leptons and neutrinos with two unitary matrices $U_L$ and $U_R$, the $U_{\mathrm{PMNS}}$ with a complete symmetry is the result, but the symmetry breaking makes both the eigenstates of lepton and neutrino undergo perturbations (equivalent to the mass matrices with certain symmetries) which correspond to $P_L$ and $P_R$. When we deduce the real physical $U_{\mathrm{PMNS}}$, such perturbations would perturb the originally symmetric mixing matrix as $P_L^\dagger U_{\mathrm{PMNS}} P_R$. Because the perturbations applied to the eigenstates of charged leptons and neutrinos may be different, it is not necessary to let them be the same. However, it is natural to simplify the picture, so that one can assume that, in general, one can just keep the eigenstates of either the charged leptons or neutrinos remaining the same as the eigenstates of weak interaction while rotating the rest ones. Thus, following the scheme adopted in the literature, for dealing only with the mixing matrix, we adopt the simplified version. As we state above, from origin, it should be $(P^L_{x,y,z})^T U_{\mathrm{PMNS}} P^R_{x,y,z}$, but, due to the simplification, we let one of $P^{L(R)}_{x,y,z}$ be a unit matrix.

Generally speaking, the perturbation to the leading order mixing matrix $U_0$ can be realized by a perturbation matrix $\Delta U$:

$$\begin{aligned} U_{\mathrm{PMNS}} &= U_0 + \Delta U = (1 + \Delta U_L) \cdot U_0 \cdot (1 + \Delta U_R) \\ &\equiv P_L^T \cdot U_0 \cdot P_R, \end{aligned} \tag{18}$$

where $\Delta U = \Delta U_L \cdot U_0 + U_0 \cdot \Delta U_R + \Delta U_L \cdot U_0 \cdot \Delta U_R$. The unitary matrices $P_{\mathrm{L/R}}$ are just three-dimensional rotations and can be a combination of the following matrices which are rotations about three independent axes:

$$\begin{aligned} P_x &= \begin{pmatrix} c_x & e^{-i\delta_x} s_x & 0 \\ -e^{i\delta_x} s_x & c_x & 0 \\ 0 & 0 & 1 \end{pmatrix}, \\ P_y &= \begin{pmatrix} 1 & 0 & 0 \\ 0 & c_y & e^{-i\delta_y} s_y \\ 0 & -e^{i\delta_y} s_y & c_y \end{pmatrix}, \\ P_z &= \begin{pmatrix} c_z & 0 & e^{-i\delta_z} s_z \\ 0 & 1 & 0 \\ -e^{i\delta_z} s_z & 0 & c_z \end{pmatrix}, \end{aligned} \tag{19}$$

where $\delta_x$, $\delta_y$, and $\delta_z$ are arbitrary phases and $s_x \equiv \sin x$, $c_x \equiv \cos x$, and $x$, $y$, and $z$ are rotation angles. Without losing generality, we consider only the minimal modifications. In this scheme we let one of $P_L$ and $P_R$ be a unit matrix, and only the other plays the role of perturbation. It should be noted that it is more purposeful to correct the constant mixing patterns from the viewpoint of the neutrino mass matrix, and, in this work, we make perturbations to these patterns formally aiming to provide information for the origin of symmetry breaking and the physics behind the mass matrix.

It should be pointed out that this preliminary work is purely focused on the mixing aspect of the neutrino. As is noted above, the mixing matrix originates from the diagonalizations of the mass matrices of the charged lepton and neutrino. Therefore, it would be more purposeful to consider the perturbation at the level of the mass matrix from the viewpoint of model building. In the basis where the charged lepton mass matrix is real and diagonal, the neutrino mass matrix $M_\nu$ can be diagonalized (assuming Majorana neutrinos) by

$$U^{\dagger}_{\rm PMNS} M_\nu U^{*}_{\rm PMNS} = {\rm Diag}(m_1, m_2, m_3), \quad (20)$$

where $U_{\rm PMNS} = U_0 + \Delta U$ and $M_\nu = M_0 + \Delta M$, i.e.,

$$(U_0 + \Delta U)^{\dagger}(M_0 + \Delta M)(U_0 + \Delta U)^{*}. \quad (21)$$

Here the correction to $U_0$ is $(U_0 + \Delta U)$, and then we can represent it as $P_L \cdot U_0 \cdot P_R$. The $M_0$ is the neutrino mass matrix at some high energy scale which can be achieved from some flavor symmetry, for instance, $A_4$, etc. $U_0$ is the corresponding unitary matrix diagonalizing $M_0$ and is transformed into the realistic lepton mixing matrix $U_{\rm PMNS}$ by the presence of $\Delta M$. Now one cannot present the analysis for the relationship between $\Delta U$ and $\Delta M$ and the transforming from $U_0$ to $U_{\rm PMNS}$ as $M_0$ to $M_\nu$; however, definitely it is the task of solving the flavor issues of massive neutrinos. One approach to exploring the structure of mass matrices is texture zero [35] or cofactor zero [36], which provides some constraints or relationships on the parameters depicting the mixing and masses of the neutrino.

In this work, we carefully analyze only the case for the tribimaximal mixing, and an explicit illustration on the results is presented by tables and figures, whereas the procedure of perturbing the remaining nine symmetric textures is similar, so we collect corresponding results in a table in the last section.

There are six possible ways to perturb the symmetric textures: $P_x \cdot U_{\rm TBM}$, $P_y \cdot U_{\rm TBM}$, $P_z \cdot U_{\rm TBM}$, $U_{\rm TBM} \cdot P_x$, $U_{\rm TBM} \cdot P_y$, and $U_{\rm TBM} \cdot P_z$. We can obtain the real $U_{\rm PMNS}$ by adjusting the parameters in $P_x$, $P_y$, and $P_z$. In Table III, we show the trigonometric functions of the mixing angles, $T_{12}$, $T_{23}$, $S_{13}$, and the Jarlskog invariant $J_{CP}$.

Before carrying out the numerical analyses we would make a discussion on the weak phase in the perturbation scenario. The strength of $CP$ violation is fully determined by the Jarlskog invariant $J_{CP} = \frac{1}{8}\cos\theta_{13}\sin 2\theta_{12}\sin 2\theta_{23}\sin 2\theta_{13}\sin\delta$, which is expressed in the standard parametrization, although it does not depend on any concrete parametrization. The phase(s) in the mixing matrix is the source of leptonic $CP$ violation and is of obvious significance. Lam and some other authors suggest that there exists a high symmetry which *a priori* demands $U_{e3} = 0$ even if it breaks, and it would result in null observation effects of $CP$ violation. Concretely, $U_{e3} = 0$, $|U_{\mu 3}|^2 = 1/2$, and $|U_{e2}|^2 = 1/3$, which manifest approximately from the neutrino oscillation data, exist in the TBM matrix obtained by considering the unitarity of the mixing matrix. This is the original *Ansatz* of TBM. Since $U_{e3} = \sin\theta_{13} e^{-i\delta}$ in the standard parametrization, $U_{e3} = 0$ implies that the Jarlskog invariant is always zero, so that there does not exist any constraint on the Dirac $CP$ phase $\delta$. Moreover, disappearance of $\delta$ in TBM is due to the vanishing $\theta_{13}$; namely, $\delta$ is "hidden" in TBM. Then the perturbation is introduced to slightly change the picture as $U_{\rm TBM} \cdot P_y$ whose results are listed in Table III to illustrate the relationship between $CP$ phase $\delta$ and perturbation phase $\delta_y$. Then, the appearance of nonzero $\theta_{13}$ induced by the perturbation $P_y$ leads to the reemergence of $\delta$. Carrying out the perturbation, $(U_{\rm TBM} \cdot P_y)_{e3} = \frac{1}{\sqrt{3}}\sin y e^{-i\delta_y}$. With $U_{e3} = \sin\theta_{13} e^{-i\delta}$ in the standard parametrization, one obtains $\sin\theta_{13} = |(U_{\rm TBM} \cdot P_y)_{e3}| = \frac{1}{\sqrt{3}}\sin y$ and $\delta = \delta_y$ once one assumes $\delta$ and $\delta_y$ fall in the interval $(0, 2\pi)$. Surely, the TBM case is only an example, whereas all ten *Ansätze* for the leptonic mixing matrix can also be presented in the table(s) in a similar way. Some detailed analyses are given in the following.

## IV. NUMERICAL ANALYSES

In this section, we analyze the numerical results obtained from the formulation derived above. In fact, the procedures for perturbing all these ten symmetric mixing patterns are analogous, so we take the tribimaximal mixing as an example and present the corresponding results of the rest in the last section.

Our strategy is the following: In the equations presented in the previous section, we let the left side $T_{ij}(S_{ij})$ be the experimentally measured value which is based on a global fit of the neutrino oscillations and listed in Table II, while the

TABLE III. The results of $T_{12}$, $T_{23}$, $S_{13}$, and $J_{CP}$ as perturbing TBM.

| TBM | $T_{12}$ | $T_{23}$ | $S_{13}$ | $J_{CP}$ |
|---|---|---|---|---|
| $P_x \cdot U$ | $2\sqrt{\frac{1+\sin(2x)\cos\delta_x}{5+3\cos(2x)-4\sin(2x)\cos\delta_x}}$ | $\cos x$ | $\frac{1}{\sqrt{2}}\sin x$ | $\frac{1}{12}\sin(2x)\sin\delta_x$ |
| $P_y \cdot U$ | $\frac{1}{\sqrt{2}}$ | $\sqrt{\frac{1+\sin(2y)\cos\delta_y}{1-\sin(2y)\cos\delta_y}}$ | 0 | 0 |
| $P_z \cdot U$ | $2\sqrt{\frac{1-\sin(2z)\cos\delta_z}{5+3\cos(2z)+4\sin(2z)\cos\delta_z}}$ | $\sec z$ | $\frac{1}{\sqrt{2}}\sin z$ | $\frac{1}{12}\sin(2z)\sin\delta_z$ |
| $U \cdot P_x$ | $\sqrt{\frac{3-\cos(2x)+2\sqrt{2}\sin(2x)\cos\delta_x}{3+\cos(2x)-2\sqrt{2}\sin(2x)\cos\delta_x}}$ | 1 | 0 | 0 |
| $U \cdot P_y$ | $\frac{1}{\sqrt{2}}\cos y$ | $\sqrt{\frac{5+\cos(2y)+2\sqrt{6}\sin(2y)\cos\delta_y}{5+\cos(2y)-2\sqrt{6}\sin(2y)\cos\delta_y}}$ | $\frac{1}{\sqrt{3}}\sin y$ | $\frac{1}{6\sqrt{6}}\sin(2y)\sin\delta_y$ |
| $U \cdot P_z$ | $\frac{1}{\sqrt{2}}\sec z$ | $\sqrt{\frac{6+3\cos(2z)-3\sqrt{3}\sin(2z)\cos\delta_z}{6+3\cos(2z)+3\sqrt{3}\sin(2z)\cos\delta_z}}$ | $\sqrt{\frac{2}{3}}\sin z$ | $\frac{1}{6\sqrt{3}}\sin(2z)\sin\delta_z$ |

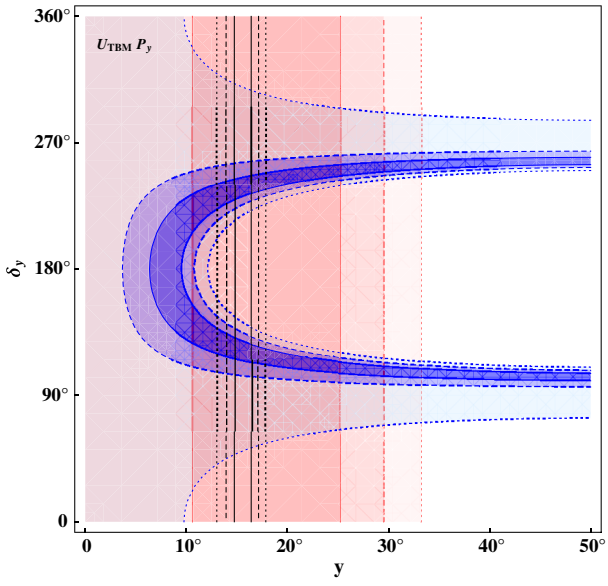


FIG. 1 (color online). The solutions corresponding to the measured $\theta_{12}$, $\theta_{23}$, and $\theta_{13}$ for the $U_{\rm TBM}\cdot P_y$ *Ansatz* in the space of parameters $y-\delta_y$. The red, light red, and pink regions correspond to the $1\sigma$, $2\sigma$, and $3\sigma$ tolerance levels of $\theta_{12}$ (data from Table II) which are divided by red solid, dashed, and dotted lines, respectively. The blue, light blue, and nattier blue regions correspond to $\theta_{23}$ for $1\sigma$, $2\sigma$, and $3\sigma$ tolerance levels of $\theta_{23}$ (Table II) which are divided by blue solid, dashed, and dotted lines, respectively. The $1\sigma$, $2\sigma$, and $3\sigma$ ranges of $\theta_{13}$ (without a special color mark in the diagram) are divided by black solid, dashed, and dotted lines, respectively.

right side is the formula we derived by perturbing the symmetric forms. Equating the two sides, we obtain several relations between the model parameters; meanwhile, we take into account the experimental errors. Plotting them in a figure (Fig. 1, for example), we have three curves which respectively satisfy the relations for $T_{12}^{\rm exp}$, $T_{23}^{\rm exp}$, and $S_{13}^{\rm exp}$. With the experimental errors, the three curves expand into three contour bands whose boundaries correspond to the error tolerance. We will observe the diagrams and see if they have overlapping regions. If there exists a common region(s) for the model parameters where all three equations are satisfied simultaneously, we would say this scheme is plausible; instead, if there is no such common region, the scheme is not successful and must be abandoned. For instance, in the case of $U_{\rm TBM}\cdot P_y$, we have

$$T_{12}^{\rm exp}=\frac{1}{\sqrt{2}}\cos y, \tag{22}$$

$$T_{23}^{\rm exp}=\sqrt{\frac{5+\cos(2y)+2\sqrt{6}\sin(2y)\cos\delta_y}{5+\cos(2y)-2\sqrt{6}\sin(2y)\cos\delta_y}}, \tag{23}$$

$$S_{13}^{\rm exp}=\frac{1}{\sqrt{3}}\sin y, \tag{24}$$

where the superscript "exp" refers to the experimental data. Solving these equations, we obtain three curves which correspond to relations between the model parameters $y$ and $\delta_y$ as shown in Fig. 1. Because of the experimental errors, the curves expand into bands. The rest of the schemes are similar, and we will not discuss the results with different perturbation *Ansätze* in every detail but show their results in the following section.

For more explicitly demonstrating the fitting effects, we provide the scatter plots. In the plots we set $\theta_{12}$, $\theta_{23}$, $\theta_{13}$, and $J_{CP}$ as horizontal and vertical axes alternatively and then mark the experimental data of the corresponding quantities, and each of them spreads into a band whose width is 3 standard deviations ($3\sigma$). There is an overlapping region where both experimental data are satisfied within $3\sigma$. Then we plot our theoretical predictions by letting the model (perturbation) parameters scan their whole allowed ranges (for example, for $U_{\rm TBM}\cdot P_y$, $0^\circ\le y\le 180^\circ$ and $0^\circ\le\delta_y\le 180^\circ$). If the theoretically predicted values which are calculated with a given perturbation *Ansatz* (the red dots) fall into the overlapping region, it means that the equation about the model parameters has solutions which coincide with the data at least within $3\sigma$ tolerance. If there are not red dots in the region, the model fails to provide a solution, so that does not work at all. Then even though in all four diagrams solutions for the model parameters seem to exist, we have to investigate if the solutions provided by the four scatter plots correspond to the same model parameter region. Indeed, the answer resides in the curved band diagrams, whereas the scatter plots can offer some detailed information about the mixing angles and $J_{CP}$ which will be measured in future experiments.

For simplicity, we take $U_{\rm TBM}\cdot P_y$ as an example to demonstrate the procedure of our numerical analyses.

For $U_{\rm TBM}\cdot P_y$ the curved bands of the three mixing angles are shown in Fig. 1. It is noted that $\theta_{12}$, $\theta_{23}$, and $\theta_{13}$ share an overlapping region within $1\sigma$. It indicates that the perturbation *Ansatz* $U_{\rm TBM}\cdot P_y$ provides a plausible scheme to accommodate all the experimental values of three mixing angles.

The scatter plots among the three mixing angles and Jarlskog invariant in the perturbation *Ansatz* $U_{\rm TBM}\cdot P_y$ are shown in Fig. 2. The $\theta_{13}-J_{CP}$ presents an upper limit of $J_{CP}$ approximately $4\times 10^{-2}$. There are large amounts of points lying in the $3\sigma$ overlapping regions of $\theta_{12}-\theta_{23}$ and $\theta_{13}-\theta_{23}$, while for $\theta_{13}-\theta_{12}$ points squeeze on a line. Even though the line deviates from the crossing point of the central values of $\theta_{13}$ and $\theta_{12}$, this line does pass through the $1\sigma$ overlapping region of $\theta_{13}-\theta_{12}$.

Whether $\theta_{23}>45^\circ$ or $\theta_{23}<45^\circ$ cannot be determined in this perturbation *Ansatz*, and the solution points are observed to be symmetric about the horizontal line $\theta_{23}=45^\circ$.

In the scatter plot of $\theta_{12}-\theta_{23}$, our calculations indicate that as $\delta_y$ varies in the range $(0,\pi/2)\cup(3\pi/2,2\pi)$ $\theta_{23}>45^\circ$, whereas $\delta_y\in(\pi/2,3\pi/2)$ we note $\theta_{23}<45^\circ$. This

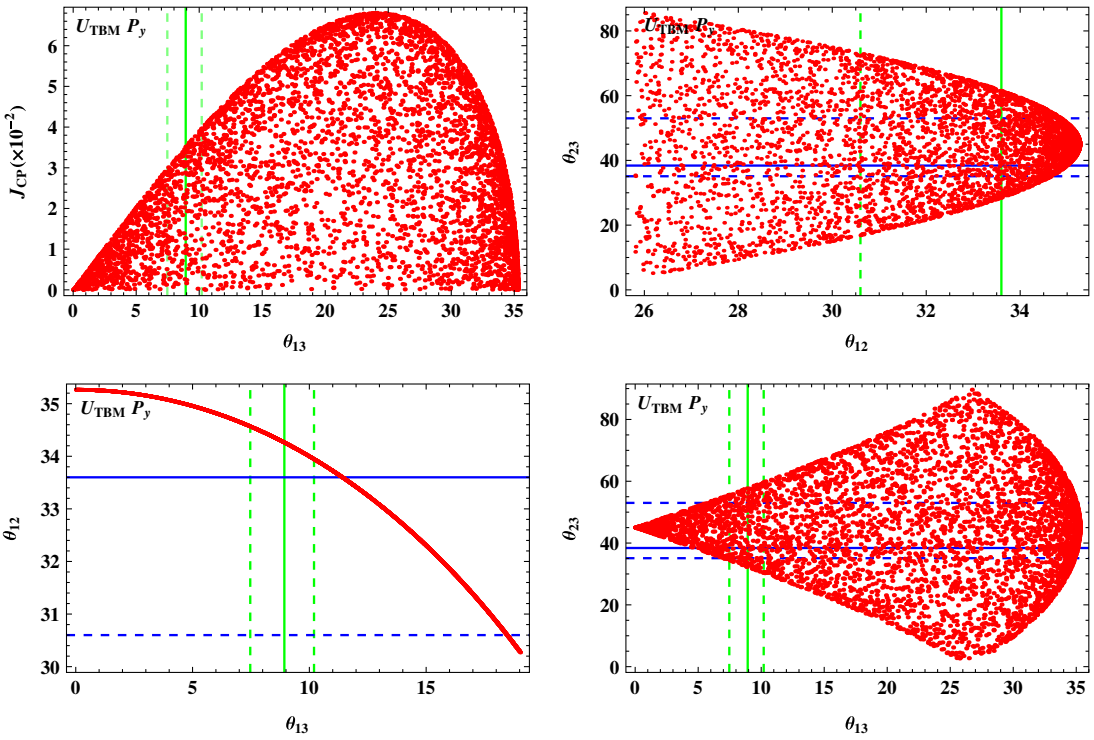


FIG. 2 (color online). The scatter plots for $\theta_{12}$, $\theta_{23}$, $\theta_{13}$, and $J_{CP}$ for $U_{\mathrm{TBM}} \cdot P_y$. The central values and $3\sigma$ ranges (by fitting the data shown in Table II) of the three mixing angles are labeled by solid lines and dashed lines, and green for the horizontal axis and blue for the ordinate one, respectively.

relationship can be confirmed by scanning the different parameter ranges of $\delta_y$ presented in Fig. 3. With the *Ansatz* $U_{\mathrm{TBM}} \cdot P_y$, $U_{e3}$ becomes

$$(U_{\mathrm{TBM}} \cdot P_y)_{e3} = \frac{1}{\sqrt{3}} e^{-i\delta_y} \sin y, \tag{25}$$

and $U_{e3}$ from the PMNS matrix in Eq. (2)is

$$(U_{\mathrm{PMNS}})_{e3} = e^{-i\delta} \sin\theta_{13}. \tag{26}$$

In this case, it is easy to get a conclusion that as $y \in (0, \pi/2)$, $\delta_y \in (0, 2\pi)$, and letting $\delta \in (0, 2\pi)$, Eqs. (25) and (26) would demand $\delta = \delta_y$. The equivalence between $\delta$ and $\delta_y$ implies that the $CP$ phase $\delta$ determines whether $\theta_{23} > 45°$ or $\theta_{23} < 45°$ or vice versa. Table II provides the $1\sigma$ range of $\delta$ (the best fit value approximately is 190°)

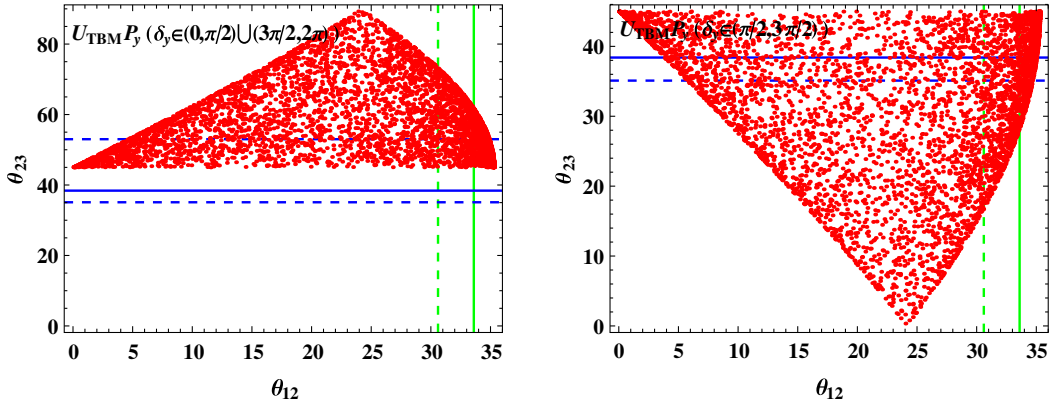


FIG. 3 (color online). The solutions corresponding to the measured $\theta_{12}$ and $\theta_{23}$ for $\delta_y \in (0, \pi/2) \cup (3\pi/2, 2\pi)$ (left panel) and $\delta_y \in (\pi/2, 3\pi/2)$ (right panel) with $y \in (0, \pi/2)$ in the perturbation *Ansatz* $U_{\mathrm{TBM}} \cdot P_z$. The central values and $3\sigma$ ranges (from the fit in Table II) of these two mixing angles are labeled by solid lines and dashed lines, green for the horizontal axis and blue for the ordinate one, respectively.

TABLE IV. The list of the results for perturbing the nine symmetric mixing textures with $P_x$, $P_y$, and $P_z$. The mark $\surd$ denotes that the corrections from the perturbation scheme make all three mixing angles consistent with data; the mark $\times$ means that, in this *Ansatz*, the calculated $\theta_{13}$ still remains as exact zero, so such an *Ansatz* does not work at all; and $\otimes$ is for the cases that the three corrected mixing angles could not be compatible with the data presented in Table II simultaneously. $\theta_{23} > 45^\circ$, $\theta_{23} < 45^\circ$, and $\theta_{23} \gtrless 45^\circ$ are marked by subscripts $S$, $L$, and $SL$, respectively. The best perturbation *Ansatz* is labeled with $\star$.

| Constant pattern | $P_x \cdot U$ | $P_y \cdot U$ | $P_z \cdot U$ | $U \cdot P_x$ | $U \cdot P_y$ | $U \cdot P_z$ |
|---|---|---|---|---|---|---|
| TBM | $\surd(\theta_{23S})$ | $\times$ | $\surd(\theta_{23L})$ | $\times$ | $\surd(\theta_{23SL})\star$ | $\surd(\theta_{23SL})$ |
| DM | $\otimes$ | $\times$ | $\otimes$ | $\times$ | $\otimes$ | $\otimes$ |
| BM | $\surd(\theta_{23S})$ | $\times$ | $\surd(\theta_{23L})$ | $\times$ | $\otimes$ | $\otimes$ |
| GRM1 | $\surd(\theta_{23S})$ | $\times$ | $\surd(\theta_{23L})$ | $\times$ | $\surd(\theta_{23SL})$ | $\surd(\theta_{23SL})$ |
| GRM2 | $\surd(\theta_{23S})$ | $\times$ | $\surd(\theta_{23L})$ | $\times$ | $\surd(\theta_{23SL})$ | $\surd(\theta_{23SL})$ |
| HM | $\surd(\theta_{23S})$ | $\times$ | $\surd(\theta_{23L})$ | $\times$ | $\otimes$ | $\otimes$ |
| TMM | $\surd(\theta_{23S})$ | $\times$ | $\surd(\theta_{23SL})$ | $\times$ | $\otimes$ | $\otimes$ |
| TFH1 | $\otimes$ | $\times$ | $\surd(\theta_{23L})$ | $\times$ | $\otimes$ | $\surd(\theta_{23SL})$ |
| TFH2 | $\surd(\theta_{23S})$ | $\times$ | $\otimes$ | $\times$ | $\otimes$ | $\surd(\theta_{23SL})$ |
| BDM | $\otimes$ | $\times$ | $\surd(\theta_{23L})$ | $\times$ | $\times$ | $\times$ |

located in $(\pi/2, 3\pi/2)$; thus, $\theta_{23}$ should be smaller than $45^\circ$ with the $U_{\rm TBM} \cdot P_y$ *Ansatz*. This implication can also be derived from the expressions of $T_{23}$ and $S_{13}$ given in Table III as

$$\tan^2\theta_{23} = \frac{1 - \sin^2\theta_{13} + 2\sqrt{2}\sin\theta_{13}\sqrt{1 - 3\sin^2\theta_{13}}\cos\delta_y}{1 - \sin^2\theta_{13} - 2\sqrt{2}\sin\theta_{13}\sqrt{1 - 3\sin^2\theta_{13}}\cos\delta_y}. \tag{27}$$

The relation indicates that $\delta_y \in (0, \pi/2) \cup (3\pi/2, 2\pi)$ requires $\theta_{23} > 45^\circ$ and $\theta_{23} < 45^\circ$ as $\delta_y \in (\pi/2, 3\pi/2)$. Equality $\delta = \delta_y$ means that $\theta_{23} \lessgtr 45^\circ$ can be determined by the $CP$ phase $\delta$ or vice versa.

## V. DISCUSSION AND CONCLUSION

The recent experiments determine a nonzero $\theta_{13}$ which is, contrary to the prediction, made by most of the symmetric textures for the lepton mixing matrix. Even though the real PMNS matrix deviates from the symmetric form, an approximate symmetry is obvious. Moreover, it is believed that the symmetric texture results from the physics at higher energy scales and is broken during its evolution to lower energy scales. To investigate what physics is at a high energy scale, we study what mechanism breaks the symmetry. Following the schemes given in the literature, we adopt the perturbation to deform the symmetric texture into the real PMNS matrix. Because the original symmetry is approximately retained, a perturbation may be a suitable choice. In this work, we perturb the ten given matrix textures which possess symmetric patterns by various *Ansätze*. Owing to the similarity in all the cases, we take the tribimaximal mixing pattern as an example to exhibit how this perturbation method applies. We summarize the results in Table IV. Various *Ansätze* by which the three mixing angles receive corrections are carefully analyzed, and their effects are marked by a tick $\surd$ or a cross $\times$ to note if the ansatz is favored or disfavored. The subscripts $S$, $L$, and $SL$ of $\theta_{23S}$, $\theta_{23L}$, and $\theta_{23SL}$ in Table IV imply that $\theta_{23}$ acquires values smaller, larger, and smaller or larger than $45^\circ$, respectively. The mark $\otimes$ signifies the situation in which the three mixing angles acquire corrections and $\theta_{13}$ is nonzero, but the *Ansatz* cannot make the theoretical values consistent with that data in Table II. We also mark the best perturbation *Ansatz* with a star symbol $\star$ in the table.

Alternative perturbation schemes have also been proposed. Let us still take the tribimaximal mixing as an example to illustrate this new scheme: $U_{\rm TBM} = R_{23}(45^\circ)\times R_{13}(0^\circ)R_{12}(\arctan(1/\sqrt{2})) = R_{23}(45^\circ)R_{12}(\arctan(1/\sqrt{2}))$, inserting perturbation matrices between $R_{23}$ and $R_{12}$, namely, $R_{23} \cdot P \cdot R_{12}$, where $P$ is a suitable perturbation $3 \times 3$ matrix. However, such a perturbation *Ansatz* cannot provide feasible mixing angles to be consistent with the experimental data. Therefore such schemes are not phenomenologically favorable.

It is observed that the relationship between $\theta_{23}$ and $\delta_i$ (or $\delta$) $(i = x, y, z)$ could fix $\theta_{23} > 45^\circ$ or $\theta_{23} < 45^\circ$; thus, more precise measurements on $\theta_{23}$ constrain the range of the $CP$ phase.

The equality $\delta = \delta_i$ $(i = x, y, z)$ is derived as $i$ is constrained in the first quadrant $i \in (0, \pi/2)$, but when it is in the second quadrant $i \in (\pi/2, \pi)$, the result would not remain the same. From our analytical equations of $J_{CP}$, $J_{CP}$ is proportional to $\sin(2i)\sin\delta_i$ (for the TMM case, this relationship does not exist), and from the standard form of the PMNS matrix (2) and definition of the Jarlskog invariant (6), we determine $J_{CP} \sim \sin\delta$. We present a relation between $J_{CP}(\delta)$ and the perturbation parameters in Table V.

TABLE V. The relationship between $J_{CP}$ $(\delta)$ and perturbation parameters $i$, $\delta_i$ $(i = x, y, z)$, with a plus $+$ for a positive $J_{CP}$ and minus $-$ for a negative one.

| $J_{CP}$ $(\delta)$ | $\delta_i \in (0, \pi/2)$ | $\delta_i \in (\pi/2, \pi)$ | $\delta_i \in (\pi, 3\pi/2)$ | $\delta_i \in (3\pi/2, 2\pi)$ |
|---|---|---|---|---|
| $i \in (0, \pi/2)$ | $+(\delta < \pi)$ | $+(\delta < \pi)$ | $-(\delta > \pi)$ | $-(\delta > \pi)$ |
| $i \in (\pi/2, \pi)$ | $-(\delta > \pi)$ | $-(\delta < \pi)$ | $+(\delta < \pi)$ | $+(\delta < \pi)$ |

Our numerical analysis indicates that the TBM is a more favorable texture that may accommodate a sizable $\theta_{13}$ after a perturbative correction. With the perturbation, $\theta_{23}$ and $\theta_{13}$ deviate from 45° and 0° as required by the data, and it means that the $\mu - \tau$ symmetry [34] originally embedded in the neutrino mass matrix is broken by the perturbation. Especially the $U_{\rm TBM} \cdot P_y$ provides the most plausible perturbation *Ansatz* for the theoretical mixing angles to be consistent with the experimental values in the $1\sigma$ level. This indicates that the most viable correction to TBM is produced by the rotation in the 2–3 plane, i.e., to break the $\mu - \tau$ symmetry [34] by a perturbation. This provides us a clue for model building in the future.

## ACKNOWLEDGMENTS

This work is supported by the National Natural Science Foundation of China under Contracts No. 11075079 and No. 11135009.

[1] H. Fritzsch, Phys. Lett. **73B**, 317 (1978); Nucl. Phys. **B155**, 189 (1979).
[2] C. S. Lam, Phys. Rev. D **83**, 113002 (2011); arXiv:1105.4622.
[3] K. Abe *et al.* (T2K Collaboration), Phys. Rev. Lett. **107**, 041801 (2011).
[4] Y. Abe *et al.* (Double-Chooz Collaboration), Phys. Rev. Lett. **108**, 131801 (2012).
[5] Y. Abe *et al.* (Double-Chooz Collaboration), Phys. Rev. D **86**, 052008 (2012).
[6] F. P. An *et al.* (Daya Bay Collaboration), Phys. Rev. Lett. **108**, 171803 (2012).
[7] D. Dwyer, in Proceedings of the Twenty-fifth International Conference on Neutrino Physics and Astrophysics, 2012, Kyoto, Japan (unpublished).
[8] L. Zhang, in Proceedings of the International Symposium on Neutrino Physics and Beyond, 2012, Shenzhen, China (unpublished).
[9] S.-B. Kim *et al.* (RENO Collaboration), Phys. Rev. Lett. **108**, 191802 (2012).
[10] J. Beringer *et al.* (Particle Data Group), Phys. Rev. D **86**, 010001 (2012).
[11] Z. Z. Xing and S. Zhou, *Neutrinos in Particle Physics, Astronomy and Cosmology* (Springer-Verlag, Berlin, 2011).
[12] B. Pontecorvo, Sov. Phys. JETP **26**, 984 (1968).
[13] Z. Maki, M. Nakagawa, and S. Sakata, Prog. Theor. Phys. **28**, 870 (1962).
[14] C. Jarlskog, Phys. Rev. Lett. **55**, 1039 (1985).
[15] D. D. Wu, Phys. Rev. D **33**, 860 (1986).
[16] A. Gando *et al.* (KamLAND Collaboration), Phys. Rev. D **83**, 052002 (2011).
[17] P. Adamson *et al.* (MINOS Collaboration), Phys. Rev. Lett. **107**, 181802 (2011).
[18] G. L. Fogli, E. Lisi, A. Marrone, D. Montanino, A. Palazzo, and A. M. Rotunno, Phys. Rev. D **86**, 013012 (2012).
[19] P. F. Harrison, D. H. Perkins, and W. G. Scott, Phys. Lett. B **530**, 167 (2002); Z. Z. Xing, Phys. Lett. B **533**, 85 (2002); P. F. Harrison and W. G. Scott, Phys. Lett. B **535**, 163 (2002); X. G. He and A. Zee, Phys. Lett. B **560**, 87 (2003); I. Stancu and D. V. Ahluwalia, Phys. Lett. B **460**, 431 (1999).
[20] H. Fritzsch and Z. Z. Xing, Phys. Lett. B **372**, 265 (1996).
[21] V. D. Barger, S. Pakvasa, T. J. Weiler, and K. Whisnant, Phys. Lett. B **437**, 107 (1998).
[22] Y. Kajiyama, M. Raidal, and A. Strumia, Phys. Rev. D **76**, 117301 (2007).
[23] W. Rodejohann, Phys. Lett. B **671**, 267 (2009).
[24] C. H. Albright, A. Dueck, and W. Rodejohann, Eur. Phys. J. C **70**, 1099 (2010).
[25] Z. Z. Xing, Phys. Rev. D **78**, 011301 (2008).
[26] R. de Adelhart Toorop, F. Feruglio, and C. Hagedorn, Phys. Lett. B **703**, 447 (2011).
[27] R. de Adelhart Toorop, F. Feruglio, and C. Hagedorn, Nucl. Phys. **B858**, 437 (2012).
[28] G. J. Ding, Nucl. Phys. **B862**, 1 (2012).
[29] J. E. Kim and M.-S. Seo, J. High Energy Phys. 02 (2011) 097; Int. J. Mod. Phys. A **27**, 1250017 (2012).
[30] L. Wolfenstein, Phys. Rev. Lett. **51**, 1945 (1983).
[31] Planck Collaboration, arXiv:1303.5076.
[32] A. Yu. Smirnov, arXiv:hep-ph/0402264; H. Minakata and A. Yu. Smirnov, Phys. Rev. D **70**, 073009 (2004); N. Li and B.-Q. Ma, Phys. Rev. D **71**, 097301 (2005).
[33] S. F. King, Phys. Lett. B **718**, 136 (2012); S. Antusch, C. Gross, V. Maurer, and C. Sluka, Nucl. Phys. **B866**, 255 (2013); I. Masina, Phys. Lett. B **633**, 134 (2006).
[34] R. N. Mohapatra and A. Yu. Smirnov, Annu. Rev. Nucl. Part. Sci. **56**, 569 (2006).
[35] H. Fritzsch and Z. Z. Xing, Phys. Lett. B **530**, 159 (2002); P. H. Frampton, S. L. Glashow, and D. Marfatia, Phys. Lett. B **536**, 79 (2002); H. Fritzsch, Z. Z. Xing, and S. Zhou, J. High Energy Phys. 09 (2011) 083.
[36] L. Lavoura, Phys. Lett. B **609**, 317 (2005); E. I. Lashin and N. Chamoun, Phys. Rev. D **78**, 073002 (2008).